Neuropharmacology 150 (2019) 70–79

Contents lists available at ScienceDirect

Neuropharmacology

journal homepage: www.elsevier.com/locate/neuropharm

Oxysterol modulates neurotransmission via liver-X receptor/NO synthase-dependent pathway at the mouse neuromuscular junctions

Kamilla A. Mukhutdinova[a], Marat R. Kasimov[a], Guzel F. Zakyrjanova[a,b], Milausha R. Gumerova[a], Alexey M. Petrov[a,b,*]

[a] Institute of Neuroscience, Kazan State Medical University, Butlerova St. 49, Kazan, 420012, Russia
[b] Laboratory of Biophysics of Synaptic Processes, Kazan Institute of Biochemistry and Biophysics, Federal Research Center "Kazan Scientific Center of RAS", P. O. Box 30, Lobachevsky Str., 2/31, Kazan, 420111, Russia

HIGHLIGHTS

- We studied the role of 24-hydroxycholesterol (24S-HCh) in neurotransmission in diaphragm.
- Long-term exposure to 24S-HCh depressed neurotransmitter release during 20 Hz stimulation.
- This was linked with decrease in synaptic vesicle recruitment to exocytosis.
- The action of 24S-HCh was mediated by increase in NO production mainly by eNOS.
- Liver X receptor antagonist completely prevented these effects of 24S-HCh.

ARTICLE INFO

Keywords:
24S-hydroxycholesterol
Oxysterols
Neuromuscular junction
Synaptic vesicle exocytosis
Liver X receptor
Nitric oxide

ABSTRACT

Elimination of brain cholesterol occurs in the form of 24S-hydroxycholesterol (24S-HCh) that may modulate physiological processes outside the brain. Here, using microelectrode recording of postsynaptic responses (end-plate potentials, EPPs) and fluorescent marker (FM1-43) for endo-exocytosis we studied the effects of prolonged application of 24S-HCh (2.5 h, 0.4 μM) on the neurotransmission in the mice diaphragm. 24S-HCh enhanced the depression of EPP amplitude (indicator of neurotransmitter release) and suppressed the FM1-43 dye unloading from nerve terminals (indicator of exocytosis) during electrical nerve stimulation at 20 Hz, without affecting miniature EPP amplitude and frequency. Comparison of the rates of neurotransmitter and FM1-43 releases suggested an increase in time required for the synaptic vesicle reuse. Additionally, 24S-HCh potentiated an increase in DAF-FM fluorescence (a NO-sensitive marker) in response to 20 Hz stimulation. All effects of 24S-HCh were completely prevented by liver X receptor antagonist. Either inhibitors of NO synthases (TRIM, cavtratin) or protein synthesis blocker counteracted the 24S-HCh-mediated enhancement in DAF-FM fluorescence, while inhibition of NO production with L-NAME or cavtratin and extracellular NO chelation suppressed the effect of 24S-HCh on FM1-43 dye loss during 20 Hz activity. Pretreatment for 5 days with inhibitor of 24S-HCh synthesis (voriconazole) had opposite effects on the FM1-43 unloading and NO synthesis. These data suggest that prolonged exposure to 24S-HCh attenuates recruitment of synaptic vesicle to exocytosis during 20 Hz stimulation acting via liver X receptor/NO-dependent signaling.

1. Introduction

Brain cholesterol turnover tightly depends on balance between synthesis and oxidation of cholesterol to 24S-hydroxycholesterol (24S-HCh) by highly conserved cytochrome P450 46A1 (CYP46A1, cholesterol 24-hydroxylase) located in endoplasmic reticulum of many neurons (Ramirez et al., 2008). 24S-HCh freely passes brain-blood barrier and then it is excreted by hepatocytes into bile. Enhanced cholesterol metabolism in the brain results in an elevation of 24S-HCh in the circulation and rate of 24S-HCh production was found to be

Abbreviations: eNOS, endothelial nitric oxide synthase; 24S-HCh, 24S-hydroxycholesterol; NMJ, neuromuscular junction; nNOS, neuronal nitric oxide synthase; LXR, liver X receptor; NO, nitric oxide

* Corresponding author. Institute of Neuroscience, Kazan State Medical University, Butlerova St. 49, Kazan, 420012, Russia.
E-mail addresses: fysio@rambler.ru, aleksey.petrov@kazangmu.ru (A.M. Petrov).

https://doi.org/10.1016/j.neuropharm.2019.03.018
Received 23 July 2018; Received in revised form 15 February 2019; Accepted 13 March 2019
Available online 18 March 2019
0028-3908/

~0.09 mg/day/kg body weight (Bretillon et al., 2000; Russell et al., 2009). Measurements of the rate of cholesterol synthesis and its conversion into 24S-HCh in rat brains suggest that ~0.02% of the total brain cholesterol is converted into 24S-HCh per hour (Björkhem I et al., 1997). The main target for 24S-HCh is nuclear liver X receptors (LXRs) which regulate genes involved in lipid metabolism and inflammatory response (Lütjohann et al., 1996; Janowski et al., 1999). Additionally, 24S-HCh might affect glutamatergic transmission and neuronal survival via positive allosteric modulation of NMDA-receptors (Paul et al., 2013; Sun et al., 2017). Despite the evident role of 24S-HCh in the central nervous system, the involvement of the oxysterol in physiological and pathological processes outside the brain remains unclear. Recently, we found that 24S-HCh at the submicromolar range can affect β1/2-adrenergic signaling in mice atria (Odnoshivkina et al., 2019). The mean plasma concentration of 24S-HCh was about 80 ng/ml (~0.2 μM) in healthy volunteers (age 24–47 years) (Babiker and Diczfalusy, 1998), but it might change significantly in aging and during the progression of some neurodegenerative diseases (Leoni and Caccia, 2013; Petrov et al., 2016). High levels of 24S-HCh were detected in infant (385 ng/ml, 1–5 years), children (258 ng/ml, 6–9 years) and teenagers (192 ng/ml, 10–18 years), which may be secondary to a high turnover of brain cholesterol during these periods of life (Bretillon et al., 2000). In case of Niemann-Pick disease, a lysosomal storage disorder, abnormal accumulation of cholesterol occurs in late endosome/lysosomes, which leads to a decrease in cholesterol availability in cellular membranes. As a results, in Niemann-Pick type C1 patients the basal level of 24S-HCh plasma levels were lower (10–30 ng/ml) and increased 1.43- to 1.75-fold at 3–8 h following intracerebroventricular injection of 2-hydroxypropyl-β-cyclodextrin, which facilitates traffic of cholesterol to endoplasmic reticulum, where cholesterol is converted into 24S-HCh (Sidhu et al., 2015). Note that in addition to psychiatric symptoms Niemann-Pick type C patients have profound motor dysfunction (Vanier, 2010).

Neuromuscular junction (NMJ) is a key point where the commands from motor neurons are translated into the muscle fibers (Slater, 2017). The synaptic transmission through NMJs has a high sensitivity to some oxidized cholesterol derivatives characterized by potential toxic or neuroprotective properties (Kasimov et al., 2015, 2016). Naturally occurring oxysterols are physiological ligands for LXRs (Janowski et al., 1999). LXRs are expressed in skeletal muscles and the number of NMJs decreases in LXRβ-deficient mice (Bigini et al., 2010). However, the role of LXRs in NMJs is poorly understood. Recently we revealed that, in the mice NMJs, 20-min exposure to 24S-HCh can potentiate synaptic vesicle exocytosis during 20 Hz stimulation and, in contrast to central synapses, counteracts the effect of NMDA-receptor activation (Kasimov et al., 2017). The same short application of 24S-HCh leads to the opposite change in the rate of synaptic vesicle exocytosis in NMJs of $SOD1^{G93A}$ mice (Mukhutdinova et al., 2018). The influence of prolonged treatment with 24S-HCh on neuromuscular communication and the involvement of LXRs in the synaptic effects of the oxysterol are unknown.

In the present study we found that 24S-HCh application lasted 2.5 h suppresses neurotransmitter exocytosis during 20 Hz stimulation in the mice NMJs. This effect of 24S-HCh is dependent on increase in NO production in response to the synaptic activity. Pharmacological inhibition of LXRs completely prevents the effects of 24S-HCh on both the synaptic vesicle exocytosis and NO synthesis.

2. Methods

2.1. Ethical approval

This study conforms to the Guide for the Care and Use of Laboratory Animals (NIH Publication No. 85–23, revised 1996) and European Convention for the Protection of Vertebrate Animals used for Experimental and other Scientific Purposes (Council of Europe No 123, Strasbourg, 1985). Isolated hemidiaphragms of adult male CD-1 mice (4–6 months of age) were used in the experiments. Animals had free access to water and food in condition of a 12-h light/12-h dark cycle. After anesthesia with an intraperitoneal injection of sodium pentobarbital (40 mg/kg) the mice were decapitated with a guillotine; the muscle with nerve stub quickly excised. The experimental protocol met the requirements of the EU Directive 2010/63/EU and was approved by the Bioethics Committees of Kazan Medical University.

2.2. Solution and chemicals

Hemidiaphragms with a phrenic nerve were attached to the bottom of a Sylgard-filled plexiglass chambers (volume, 3 ml). The preparations were constantly superfused at 5 ml·min^{-1} with physiological solution saturated with a 5% CO_2/95% O_2 mixture and containing (in mM): NaCl (129.0), KCl (5.0), $CaCl_2$ (2.0), $MgSO_4$ (1.0), NaH_2PO_4 (1.0), NaHCO3 (20.0), glucose (11.0) and HEPES (3.0). pH was maintained at 7.4 at 23-24^{0}C.

Application of 24S-HCh (Enzo Life Sciences) lasted 2.5 h before motor nerve stimulation at 20 Hz. DMSO (Tocris) was used as dissolving agent (10 mg/ml) and its final concentration in the bath solution was ≤0.001%. At a concentration of 0.001% DMSO did not modify any of the recorded parameters, consistent with our previous studies (Kasimov et al., 2017; Mukhutdinova et al., 2018). The data from DMSO controls were pooled with DMSO-free controls into one group.

GSK 2033 (10 μM; 2,4,6-Trimethyl-*N*-[[3'-(methylsulfonyl)[1,1′-biphenyl]-4-yl]methyl]-*N*-[[5-(trifluoromethyl)-2-furanyl]methyl]benzenesulfonamide; liver X receptor antagonist, Tocis), L-NAME, (100 μM; Nω-Nitro-L-arginine methyl ester hydrochloride; inhibitor of NO synthases; Sigma), cavtratin (5 μM; caveolin-1 scaffolding domain peptide endothelial NO synthase blocker; Enzo Life Sciences), TRIM (30 μM; 1-(2-Trifluoromethylphenyl)imidazole; inhibitor of neuronal and inducible NO synthases; Tocris), cycloheximide (200 μM; 4-[2-(3,5-Dimethyl-2-oxo-cyclohexyl)-2-hydroxyethyl]-2,6-piperidinedione; blocker of protein synthesis, Tocris) were added to the perfusion 15 min before exposure to 24S-HCh and remained in the bath throughout the experiment. AP-5 (25 μM; D-2-amino-5-phosphonovaleric acid, NMDA-receptor competitive antagonist, Sigma) was co-applied with 24S-HCh. Donor NO, DEA NONOate (100 μM Diethylamine NONOate diethylammonium salt, Sigma), was added into the bathing solution 2 min prior to FM1-43 unloading, because it releases NO which has a relatively short live-time in solution. Also, hemoglobin (Hb; an extracellular NO scavenger; Sigma) was added into the perfusion solution (final concentration of 30 μM) 5 min before onset of FM1-43 unloading stimulation. GSK 2033, cavtratin, TRIM and voriconazole were dissolved in DMSO with the concentrations 11, 30, 10 and 33 mg/ml in stock solutions, respectively. The stock solutions were stored as aliquots for a maximum 3 weeks. L-NAME, cycloheximide, AP-5, DEA NONOate were dissolved in saline prior to experiment. After adding any of these compounds (in corresponding concentrations) together with 24S-HCh (0.4 μM) the final DMSO concentration in physiological solution was less than 0.08%. At a concentration of 0.1% DMSO also did not affect the measured parameters (Suppl. Table 1).

Pretreatment with voriconazole. Animals were injected with voriconazole (Sigma) for 5 days (intraperitoneally, 60 mg/kg/day). This protocol leads to reduce plasma levels of 24S-HCh by around 30% (Shafaati et al., 2010). The control mice were treated with the voriconazole-free physiological solution. Additionally, some control isolated muscles were exposed to 1 μM voriconazole for 2.5 h (acute treatment).

2.3. Electrophysiology

The postsynaptic end-plate potentials (EPPs) and miniature EPPs (MEPPs) were recorded with one standard intracellular glass microelectrodes (with a tip resistance of 25–30 MΩ, filled with 2.5 M KCl;

without current injection) using bridge balance circuit and a 0.5–2 kHz band-pass filter. The registered signals were digitized at 50 kHz and stored on PC for off-line analysis (Kasimov et al., 2015, 2017). Recording equipment consisted of a Model 1600 (A-M System) amplifier and LA II digital I/O board (Pushino, Russia). Data were acquired and processed using a custom-developed program (developed by PhD Zakharov A.V.) and analyzed offline to calculate mean amplitudes, rise times (from 20% to 80% of the peak amplitude), decay time constants (from peak to 50% of the peak amplitude), using Origin software. The motor nerve was stimulated by supramaximal electrical 0.1-ms pulses with a suction electrode connected to DS3 stimulator (Digitimer Ltd.). We applied either a low-frequency stimulation (0.2 Hz) or 20 Hz stimulation (for 3 min) to the nerve. To estimate effect of 24S-HCh, MEPPs or EPPs (at 0.2 Hz) were recorded during 10–15 min from 12 to 15 different muscle fibers before and after perfusion with 24S-HCh-free or -containing physiological solution. At least 12–15 MEPPs or 4–5 EPPs were recorded in the individual muscle fiber. The data from individual muscle fibers were then pooled to obtain average values of the MEPP and EPP parameters before and after 24S-HCh application in the muscle. To avoid muscle contractions, the muscle-specific Na^+ channel blocker μ-conotoxin-GIIIB (0.5 μM; Alamone Lab) was added to the bathing solution 20 min prior to recording.

2.4. Fluorescence microscopy

Fluorescence images were captured using an Olympus BX51WI microscope equipped with confocal attachment Disk Scanning Unit and UPLANSapo 60xw/LumPlanPF 100 × w objectives. Images were recorded with CCD cameras (DP71, Olympus and Orca R2, Hamamatsu) under control Cell^P software (Olympus). Multiple optical sections in the z-axis were acquired using an ECO-MOT focus stepper. Using ImagePro software (Media Cybernetics), intensity analysis was made on regions of interest in arbitrary units (a.u.), which were then converted into percentages.

2.4.1. Imaging of synaptic vesicle exocytosis in motor nerve terminals

FM1-43 dye (7 μM; Thermo Fisher) was used to estimate the rate of synaptic vesicle exocytosis. FM1-43 reversibly binds to the plasma membranes and becomes trapped into the synaptic vesicles during endocytosis (Betz and Bewick, 1993; Ribchester et al., 1994). To load FM1-43 into the nerve terminals, the motor nerve was stimulated at 20 Hz for 1 min. FM1-43 was added in the external solution 1 min before the onset of stimulation and the dye was present in the bath during and 5 min after 20-Hz stimulation. The preparations were then perfused with ADVASEP-7 (3 μM; Biotium)-containing solution for 20 min to facility dissociation of FM1-43 from the surface non-endocytosed membranes. After exposure of the muscle to the chemicals (including 24S-HCh), the motor nerve was re-activated at 20 Hz to evoke synaptic vesicle fusion, which causes a decrease in the nerve terminal fluorescence (unloading). Fluorescent images were captured immediately prior to onset of 20 Hz stimulation (0) and at different time points (5, 10, 15, 20, 25, 30, 45, 60, 90, 120, 150, 180, 240, 300, 420, 600 s) during 20 Hz stimulation. The NMJs were illuminated only in moments of the image capturing.

FM1-43 fluorescence was recorded using a 480/20 nm excitation filter, a 505 nm dichroic mirror and a 535/40 nm emission filter. Background fluorescence was calculated as the average intensity in a region outside of the NMJs (4x20 μm^2). Nerve terminal fluorescence was defined as the mean pixel intensity in regions of interest after background fluorescence subtraction (see Petrov et al., 2008, for details). To represent the kinetics of FM1-43 loss, the initial nerve terminal fluorescence (immediately before onset of stimulation) was taken as 1.0.

2.4.2. Estimation of synaptic vesicle reuse

FM1-43 destaining curves provide an indication of the number of synaptic vesicles that lose the dye during exocytosis. After the fusion events, both neurotransmitter and FM1-43 escape from the exocytosed vesicles and retrieved vesicles uptake little or no FM1-43. Fusion of the recycled vesicles during ongoing stimulation will lead to neurotransmitter release, but no decrease in the FM1-43 fluorescence in the nerve terminal. The summed EPP amplitude curves indicate the amount of acetylcholine released as a result of all exocytotic events. In the initial time points the rates of FM1-43 dye and neurotransmitter release are similar, but synaptic vesicle recycling will lead to lag the rate of FM1-43 unloading compared to rate of neurotransmitter release. The inverted FM destaining curve (indicator of FM1-43 release rate) was scaled to fit the summed EPP amplitude curve (indicator of neurotransmitter release) at early times after onset of stimulation (at least first 10 s), when FM1-43 and neurotransmitter releases occur at the same rate. These curves superimposed well at early times, but diverged later due to neurotransmitter release from the dye-free recycling vesicles. In the case of faster/slower vesicle recycling more/less scaling of the inverted FM unloading curve is required to fit the summed EPP curve. This superposition of the scaled inverted FM1-43 unloading curve and the cumulative EPP amplitude curve allows to estimate roughly the mean dead-end time of synaptic vesicle reuse (Betz and Bewick, 1993; Petrov et al., 2008). The time is defined by the point of discrepancy of the curves, i.e. when the dye-loss rate starts to lag compared to the rate of neurotransmitter release. Gap between the curves in 15% of the curve divergence at the end of 20 Hz stimulation was set as arbitrary criteria of the curve discrepancy time.

2.4.3. Detection of nitric oxide (NO)

Generation of NO oxidation products was visualized using a DAF-FM-diacetate (Thermo Fisher). DAF-FM fluorescence was excited by a 488/10 nm wavelength light and detected using an emission filter that transmits 505–560 nm; a 505 nm dichroic mirror was used. The hemidiaphragms were exposure to 4 μM DAF-FM-diacetate for 20 min and then were perfused for 40 min with the dye-free physiological solution before measurements of the fluorescence in NMJs. Additionally, postsynaptic nicotinic acetylcholine receptors were labeled with rhodamine-conjugated α-bungarotoxin (Btx, 30 ng/ml; Thermo Fisher), which was added simultaneously with DAF-FM diacetate. Red fluorescence of Btx was excited by 555/15 nm wavelength light and emission was detected with a 610–650 nm filter; a 575 nm dichroic mirror was used. The analysis of DAF-FM fluorescence intensity was made in regions of interests (surface junctional and extrajunctional areas). Junctional fluorescence was defined as mean pixel intensity in Btx-positive region. Extajunctional fluorescence was estimated in area (10 × 20 μm^2) outside Btx-stained NMJs. The value of the initial fluorescence in region of interest was taken as 1.0. To control photobleaching of DAF-FM during fluorescence recording, we measured the fluorescence intensity without stimulation at the same conditions of illumination as when the preparations were stimulated to induce activity-dependent increase in DAF-FM fluorescence. Treatments with the chemicals were started immediately after the end of the dye application.

2.5. qRT-PCR

Total RNA (1 μg for each sample) was isolated from the diaphragm with TRIzol™ isolation reagent according to the manufacturer's instruction (Thermo Fisher). Then the RNA was converted to cDNA by SuperScript III Reverse Transcriptase (Thermo Fisher) and analyzed with a qRT-PCR detection system (Bio-Rad). The sequences of primers for gene quantification were taken from qPrimerDepot, a primer database (Cui et al., 2007). PCR reactions for each sample (from individual mouse) were conducted in triplicate. All the expression levels were normalized to expression of beta-actin. Primer quality was checked.

2.6. Statistical analysis

Statistical analysis was made using Origin Pro 9.2 software, assuming a significance level of 0.05. The data are presented as Mean ± S.E.M., where n is the number of independent experiments on different mice, with statistical significance assessed by the Student's *t*-test or repeated one–way ANOVA (for parametric data) followed by the Bonferroni post-hoc test and Mann-Whithey test (for non-parametric data).

3. Results

3.1. Prolonged application of 24S-HCh suppresses both neurotransmitter release and FM1-43 unloading during stimulation at 20 Hz

Initially, we recorded resting membrane potential and postsynaptic potentials which reflect spontaneous (MEPPs) and evoked (EPPs at 0.2 Hz) neurotransmitter release before and after 24S-HCh (0.4 μM) application lasted 2.5 h. The mean resting membrane potential of muscle fibers was 75.3 ± 1.7 mV before and 74.4 ± 1.5 mV after the incubation with 24S-HCh (n = 15 animals; 210 muscle fiber). Additionally, there were no differences in MEPP rise (0.79 ± 0.03 vs 0.77 ± 0.04 ms) and decay (3.22 ± 0.11 vs 3.15 ± 0.14 ms, n = 7 animals; 96 muscle fibers) times. These data suggest no marked changes in properties of muscle fiber membranes. Neither the MEPP amplitude nor frequency was significantly affected by 24S-HCh (n = 7 animals; 96 muscle fiber). In addition, 24S-HCh had no influence on the EPP amplitude, rise or decay-times (n = 8 animals; 105 muscle fibers) (Fig. 1A). Since the MEPP and EPP amplitudes were virtually unchanged, exposure to 24S-HCh does not modulate neurotransmitter release triggered by low frequency stimulation (0.2 Hz). Such pattern of activity leads to release of neurotransmitter stored within a small population of synaptic vesicles belonging to the ready releasable pool (Slater, 2017).

Stimulation of a motor nerve at higher frequencies, that resembles *in vivo* activity, recruits synaptic vesicle from the recycling and reserve pools. Under these conditions, the efficiency of neurotransmitter release is dependent on the translocation of synaptic vesicles to the exocytotic sites and their reuse during continuous stimulation (Maeno-Hikichi et al., 2011). After 2.5-h application of 24S-HCh, 20 Hz stimulation resulted in a more profound drop in the EPP amplitude (to 36.0 ± 2.7% by the 3rd min of stimulus train, p < 0.01, n = 8 animals) compared with the control (the amplitude decline to 56.9 ± 3.0%, n = 9 animals) (Fig. 1B). The cumulation of EPP amplitudes provide a measure of summed action potential-evoked neurotransmitter release at 20 Hz stimulation for 3 min (Fig. 1C). The evident differences in the cumulative curve slopes suggest that 2.5 h treatment with 24S-HCh significantly decreased total neurotransmitter release for 3 min of 20 Hz stimulation and the discrepancy between the curves increased during the stimulation. Eventually, exposure to 24S-HCh significantly decreased the summed EPP amplitude by 24 ± 4% (P < 0.001) at the end of the stimulus train.

NMJs were loaded with FM1-43 dye (see Methods) and after 2.5 h-rest period the motor nerves were re-stimulated to detect the escape of the FM1-43 dye from synaptic vesicles during evoked exocytosis. Exposure of FM1-43 pre-loaded NMJs to 24S-HCh itself (without stimulation, for 2.5 h; rest conditions) did not affect nerve terminal fluorescence (n = 11) compared to the control (n = 14 animals), indicating no change in the dye loss due to spontaneous (action potential-independent) exocytosis (Fig. 2A). However, 24S-HCh reduced the rate of FM1-43 unloading at 20 Hz stimulation and the nerve terminal fluorescence decreased to 51.3 ± 2.8% (n = 11 animals, p < 0.05 versus 42.1 ± 3.1% in the control, n = 14 animals) after 3 min of stimulation (Fig. 2B). Thus, prolonged treatment with 24S-HCh did not modulate spontaneous exocytosis, but suppressed enhancement of synaptic vesicle exocytosis induced by 20 Hz stimulation. Probably, 24S-HCh could decrease the involvement of FM1-43-containing vesicles in exocytosis in response to 20 Hz stimulation.

To exclude the influence of 2.5 h incubation with 24S-HCh on FM-dye photostability during FM1-43 unloading protocol, the FM1-43 fluorescence (without stimulation) was recorded at the same conditions of illumination as when the NMJs were stimulated to unload the FM1-43. The FM1-43 fluorescence was not significantly changed on the time scale of the stimulation used for FM1-43 unloading in the control and 24S-HCh-treated muscles (Suppl. fig. 1).

Time course of synaptic vesicle reuse is dependent on duration of all steps constituting presynaptic vesicle cycle. By comparing summed EPP amplitude and inverted FM1-43 unloading curve, the time of vesicle recycling was estimated (see Methods). The curves were superimposed and scaled to fit in the initial time points, when the fluorescent dye and neurotransmitter releases occur at the same rates. The divergence of these curves was observed later in 24S-HCh-treated NMJs versus the control NMJs. This means that the rate of FM1-43 unloading begins to lag behind the rate of neurotransmitter release at later time than of control. The discrepancy between the curves could be caused by synaptic vesicle reuse during synaptic activity and suggests that the 24S-HCh suppresses the recycling during 20 Hz stimulation (Fig. 2C). Theoretically, the reduction of release probability could decrease a number of synaptic vesicles reused during a 20 Hz stimulation, affecting thereby the estimation of vesicle recycling. But, 24S-HCh did not modulate pair-pulse facilitation, indicating no changes in neurotransmitter release probability (Suppl. fig. 2).

3.2. Time-dependent effect of 24S-HCh on FM1-43 unloading

Duration of 24S-HCh application determines the outcome of the

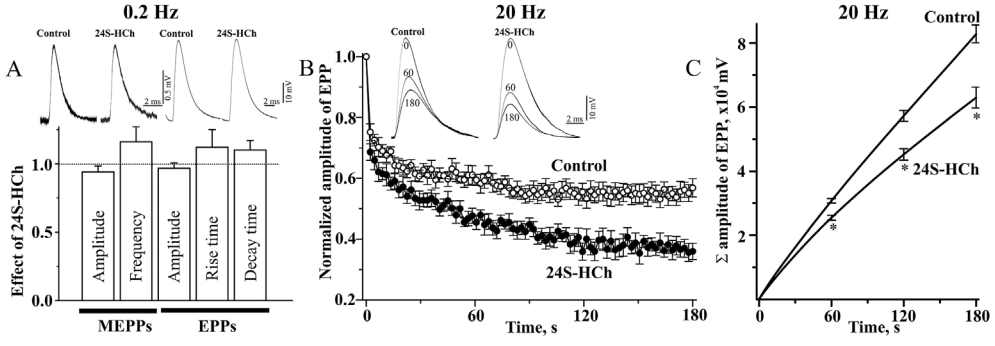

Fig. 1. Influence of prolonged 24S-HCh application on the neurotransmitter release. A – Top, typical MEPPs and EPPs (at 0.2 Hz) before and 2.5 h after exposure to 24S-HCh. To elicit EPPs, the motor nerve was simulated at low frequency. Bottom, the histogram showing the effects of the 24S-HCh treatment on peak amplitude and frequency of MEPPs (left), and key parameters of EPPs (right). No significant changes were revealed in MEPPs/EPPs under these conditions. Y-axis indicates the normalized effect of 24S-HCh (1.0 – is a value before exposure to the oxysterol). B - Changes in the neurotransmitter release during 20 Hz stimulation. Decline in EPP amplitude at 20 Hz stimulation is shown for control and 24S-HCh-treated neuromuscular junctions. Top, typical EPPs at 0, 60 and 180s of 20 Hz stimulation of the motor nerve. Bottom, data are expressed as the relative changes from the initial value (1.0) obtained immediately prior to onset of the stimulation. After treatment with the oxysterol the depression of EPP amplitude during 20 Hz activity was markedly attenuated. C-Cumulative curves of EPP amplitudes (in mV) during the 20 Hz stimulation. *Asterisks display significant differences (P < 0.001) versus control.

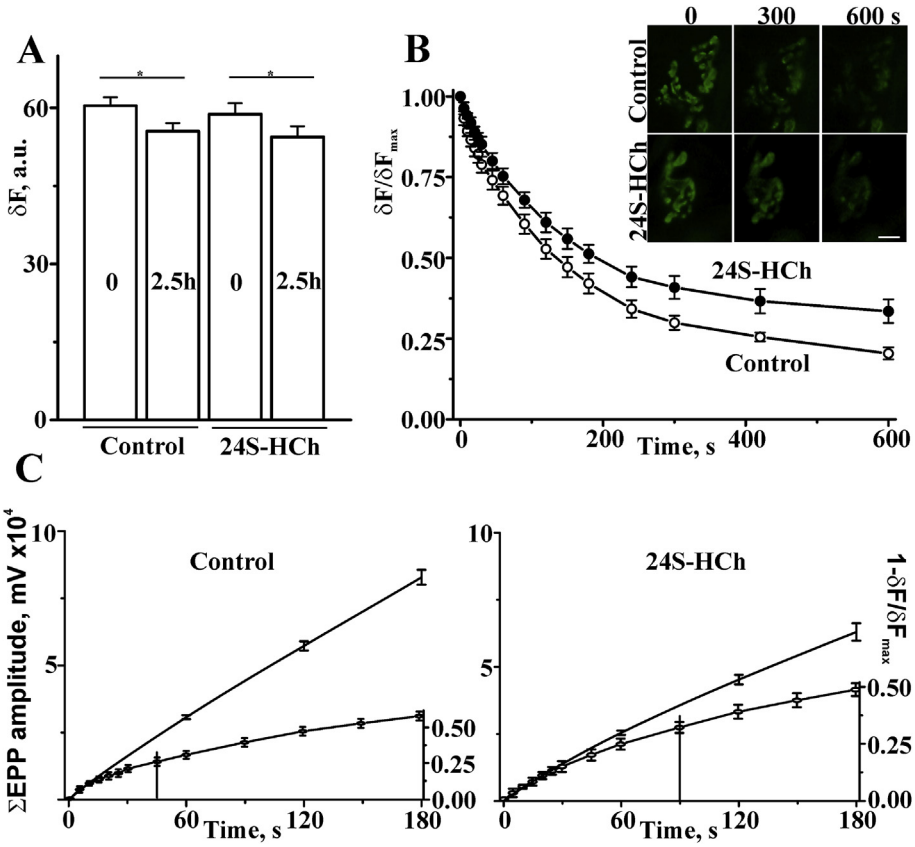

Fig. 2. Influence of 24S-HCh on FM1-43 unloading and synaptic vesicle recycling time. A- After loading with FM1-43 dye the neuromuscular junctions were perfused during 2.5 h with 24S-HCh-free or 24S-HCh-containing physiological saline. At the end of this period, the intensity of the nerve terminal fluorescence slightly decreased (*P < 0.01 compared to the initial value) to a similar degree in 24S-HCh-treated and non-treated muscles, indicating that the oxysterol did not change release of the dye by spontaneous exocytosis. Y-axis - the fluorescence in arbitrary unit after subtraction background fluorescence (δF, a.u.). B- Time course of FM1-43 unloading during 20 Hz stimulation. After the treatment with 24S-HCh, the motor nerve was re-stimulated to evoke massive exocytosis which causes release both neurotransmitter and FM1-43 molecules from synaptic vesicles. These curves indicate that 24S-HCh suppresses the rate of FM1-43 unloading. Insert, typical fluorescent images before (0) and during (300, 600 s) stimulation; scale bar – 10 μm. Y-axis – the normalized fluorescence intensity, relative to the value prior to the onset of stimulation (δF/δFmax). C – Estimation of average vesicle recycling time at 20 Hz stimulation. The inverted FM1-43 unloading curve (from Fig. 2B) was scaled to fit the initial part of the cumulative EPP amplitude curve (from Fig. 1C). These curves superimposed well at early time (at least the first 15 s), but clearly diverged later (marked by arrow). This graph indicates that 24S-HCh increases the average time required for the vesicle reuse. The scales of right Y are different, because for this comparison each inverted FM1-43 unloading curve was scaled separately from other to superimpose on the corresponding cumulative curve of EPP amplitude.

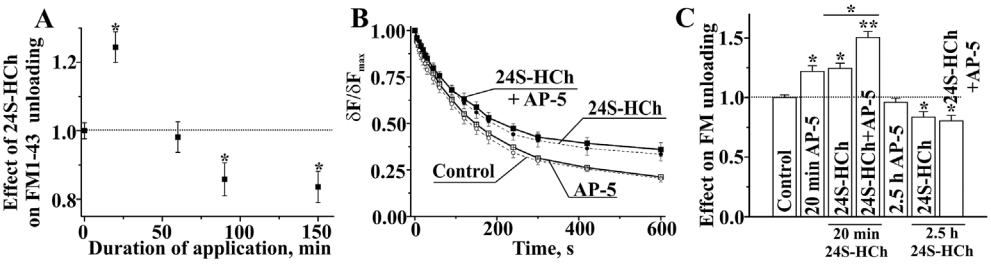

Fig. 3. Time-dependence of 24S-HCh effects on FM1-43 dye unloading. Role of NMDA-receptors. A- Graph showing change in FM1-43 loss from nerve terminals 3 min after 20 Hz-stimulation in muscles treated with 24S-HCh for different time. Y-axis – normalized effect of 24S-HCh (1.0 – is the amount of FM1-43 fluorescence loss in the control muscles at the end of 3 min of the stimulation). X-axis – duration (in min) of 24S-HCh application. These data indicate that short and long applications of the oxysterol had opposite effects on the dye release during stimulation at 20 Hz *Asterisks denote significant differences (P < 0.05) versus the control. B- Comparison of the FM1-43 unloading curves in muscles perfused for 2.5 h with 24S-HCh-free and -containing physiological solutions in the presence of glutamate NMDA-receptor antagonist (AP-5). The FM-1-43 unloadings in control and 24S-HCh-treated muscles (from Fig. 2B) are shown by dashed lines. C – Histogram illustrating the effect of NMDA-receptor antagonist (AP-5) on change in FM1-43 unloading in response to treatment with 24S-HCh for 20 min and 2.5 h. Shown effects of 20 min and 2.5 h applications of AP-5, 24S-HCh and co-application AP-5 and 24S-HCh. Y-axis is normalized effect; FM1-43 unloading 3 min after 20 Hz stimulation was taken as 1.0. B,C - The inhibitor of NMDA-receptors modifies the action of short but not long-term application of 24S-HCh.

treatment on synaptic vesicle exocytosis at 20 Hz activity. Relatively short exposure to 24S-HCh (20 min) significantly increased the rate of FM1-43 unloading (Kasimov et al., 2017). Extension of application to 1 h led to the loss of the stimulatory effect of 24S-HCh. Moreover, after 1.5 h-treatment with 24S-HCh the rate of FM1-43 unloading was decreased (Fig. 3A). Thus, shifting from short to long-term application reverses the effect of 24S-HCh on the dye exocytosis. This might reflect the involvement of different receptor types in the response to short and long-term treatment with 24S-HCh. Previously we have found that effect of the short application of 24S-HCh was augmented by inhibition of NMDA-receptor with AP-5 (Kasimov et al., 2017). However, the influence of 2.5 h treatment with 24S-HCh was not changed by AP-5 (n = 8 animals for each group AP-5 versus AP-5 + 24S-HCh) (Fig. 3B and C). This indicates that other than NMDA-receptors are implicated in the effect of prolonged treatment with 24S-HCh. Note that, 20 min exposure to AP-5 enhanced the rate of FM1-43 unloading, while 2.5 h perfusion with AP-5 had no effect on the FM1-43 unloading. This could reflect the lack of activation of NMDA-receptor during 20 Hz activity probably due to exhaustion of glutamate precursor release after 2.5 h. Thus, the effect of 20 min application of 24S-HCh is NMDA-receptor-dependent, while the effect of 2.5 h application of 24S-HCh is NMDA-receptor independent.

3.3. The effect of 24S-HCh on neurotransmitter release and exocytosis depends on LXRs

Many oxysterols, including 24S-HCh, can affect cellular functions via binding to LXRs that regulate transcription of genes important for

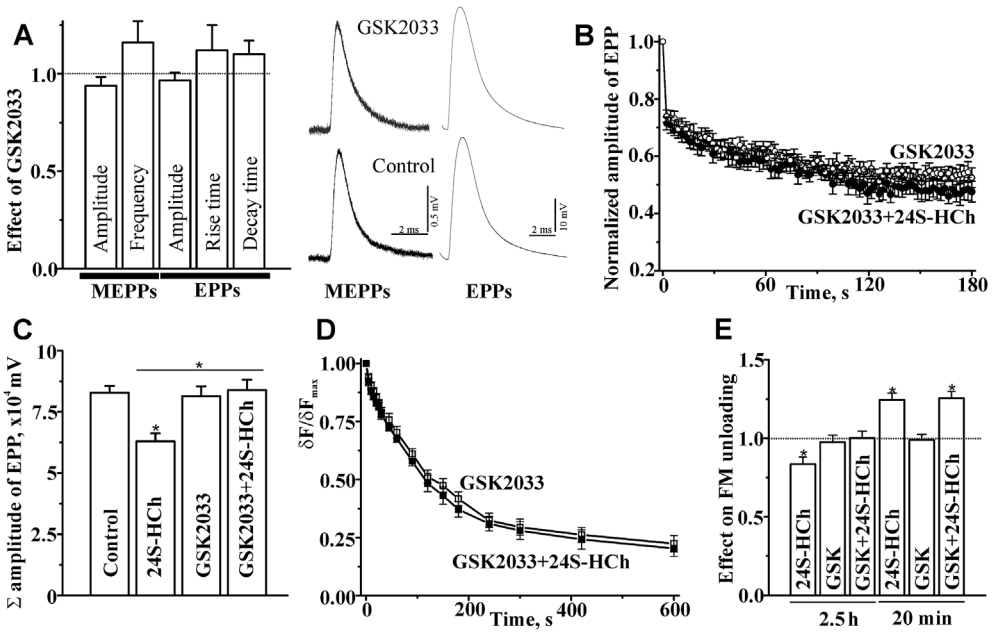

Fig. 4. Inhibitor of LXR suppresses the effects of prolonged 24S-HCh application. A – influence of GSK 2033, LXR antagonist, on spontaneous and evoked neurotransmitter release. Left, histogram showing the effect of GSK2033 on parameters of MEPPs and EPPs; right, typical MEPPs and EPPs. B – Time course of EPP amplitude during 20 Hz stimulation. Application of 24S-HCh (2.5 h) did not affect the depression of EPP amplitude when LXRs were blocked. C – Cumulative EPP amplitude (in mV) in response to 20 Hz-stimulus train lasting 3 min (from Figs. 1B and 4B). Inhibition of LXRs itself had no influence on the summed EPP amplitude, but prevented the effect of the long-term treatment with 24S-HCh. D- Kinetics of FM1-43 dye loss during stimulation at 20 Hz. Antagonist of LXRs prevented the change in the FM1-43 unloading in NMJs exposed to 24S-HCh for 2.5 h. E –Histogram illustrating the normalized effect of the oxysterol on FM1-43 destaining 3 after 20 Hz stimulation compared to the loss of FM1-43 fluorescence in the control. Thus, the effect of long (but not short) application of 24S-HCh was dependent on inhibition of LXR by GSK 2033. Asterisks display significant differences ($P < 0.05$ versus control). Other details are as in Fig. 3.

lipid metabolism and inflammatory response. Antagonist of LXRs GSK2033 (10 μM) by itself had no significant influence on MEPP amplitude (n = 7 animals, 90 muscle fibers) and EPP amplitude (n = 8 animals; 98 muscle fibers) evoked by 0.2 Hz stimulation (Fig. 4A). Also, GSK2033 did not change the EPP amplitude rundown during continuous activity at 20 Hz (n = 9 animals), but it completely prevented the effect of long-term application of 24S-HCh on the decay of neurotransmitter release at 20 Hz stimulation (n = 9 animals) (Fig. 4B). Estimation of the summed EPP amplitudes suggests that in the presence of GSK2033 treatment with 24S-HCh lost the ability to decrease total neurotransmitter release during 20 Hz activity (Fig. 4C).

Optical detection of synaptic vesicle exocytosis also supports the idea about the involvement of LXRs in the effect of prolonged application of 24S-HCh. Pharmacological inhibition of LXRs abolished the 24S-HCh-mediated decrease in the rate of FM1-43 dye loss from the dye-preloaded NMJs (n = 12 animals), while exposure to GSK 2033 alone (for 2.5 h) had no effect on the kinetics of FM1-43 unloading (n = 12 animals) (Fig. 4D). Note that effect of short-term application (20 min) of 24S-HCh was completely preserved when LXRs were blocked by GSK 2033 (n = 8/8 animals) (Fig. 4E).

These data show that prolonged exposure to 24S-HCh via activation of LXRs may result in decreased synaptic vesicle recruitment to the active zone and their recycling during 20 Hz activity. Thus, the effect of short-term application of 24S-HCh is LXR-independent, while the effect of 2.5 h application of 24S-HCh is LXR-dependent.

3.4. The exposure to 24S-HCh potentiates activity-induced enhancement of NO synthesis in a LXR-dependent manner

Previously we found that short-term application of 24S-HCh enhanced the synaptic vesicle exocytosis during 20 Hz stimulation due to an attenuation of NO synthesis at the NMJs (Kasimov et al., 2017). In contrast, prolonged exposure to 24S-HCh, that suppresses exocytosis under conditions of intense synaptic activity, potentiated an increase in NO-sensitive dye (DAF-FM) fluorescence in response to 20 Hz stimulus train in the synaptic region. The intensity of the fluorescence increased to 38.6 ± 3.1% (n = 12 animals, $P < 0.05$ versus 23.1 ± 3.3% in the control, n = 14 animals) (Fig. 5A). This 24S-HCh-mediated enhancement in fluorescence was completely suppressed by the antagonist of LXRs. In this case, the fluorescence increased by 20.2 ± 2.6% (n = 11 animals, $P > 0.05$, compared with NMJs treated with GSK2033 alone, n = 11 animals) (Fig. 5B). Notably, DAF-FM fluorescence in extrajunctional region was not affected by 24S-HCh treatment (Suppl. Fig. 3), suggesting synapse-specific effect of 24S-HCh.

Note that an inhibition of NO synthesis with L-NAME (an antagonist of all NO synthase isoforms) prevented 24S-HCh-mediated attenuation of FM1-43 dye loss during 20 Hz stimulation (Fig. 5C). L-NAME itself increased the rate of the dye unloading and the nerve terminal fluorescence decreased to 32.2 ± 1.7% (n = 10 animals, $P < 0.05$) by 3rd min of 20 Hz stimulation. Under conditions of NO synthase inhibition, 24S-HCh had no additional influence on the rate of FM1-43 destaining (n = 10 animals) (Fig. 5C). Similarly, extracellular NO scavenger hemoglobin (Hb) enhanced the FM1-43 unloading (the fluorescence decreased to 33.2 ± 1.5% by 3rd min of the stimulation; n = 8 animals, $P < 0.05$) and blocked the effect of 24S-HCh (n = 7 animals) (Fig. 5D). On the other hand, a donor of NO (DEA NONOate) attenuated the FM1-43 unloading during 20 Hz stimulation (the fluorescence decreased to 55.5 ± 2.0% by 3rd min, $P < 0.05$, n = 8 animals) and markedly potentiated the depressant effect of 24S-HCh on the FM dye loss (the nerve terminal fluorescence fell down to 69.0 ± 3.0% by 3rd min, $P < 0.05$, n = 8 animals) (Fig. 5E).

Collectively, these results suggest that long-term treatment with 24S-HCh might suppress synaptic vesicle exocytosis during 20 Hz activity by potentiating NO production in the synaptic region. The latter is dependent on LXR activation by the oxysterol and the main source of NO is located outside the presynaptic nerve terminals.

3.5. Inhibitors of NO synthases and protein synthesis counteract the effect of 24S-HCh on NO production

To exam the source of NO, the isoform-specific inhibitors of NO synthases (NOS), TRIM (an antagonist of neuronal (nNOS) and inducible isoforms) and caveolin-1 scaffolding domain peptide cavtratin (an antagonist of endothelial isoform, eNOS), were applied (Fig. 6A and B). Exposure to TRIM (n = 11 animals) or cavtratin (n = 11 animals) partially reduced the increase in DAF-FM fluorescence at 20 Hz stimulus train. TRIM was relatively more effective than cavtratin. At the same time, treatment with TRIM partially suppressed the effect of long-term application of 24S-HCh on the enhancement of DAF-FM fluorescence during stimulation at 20 Hz (Fig. 6A), whereas treatment with

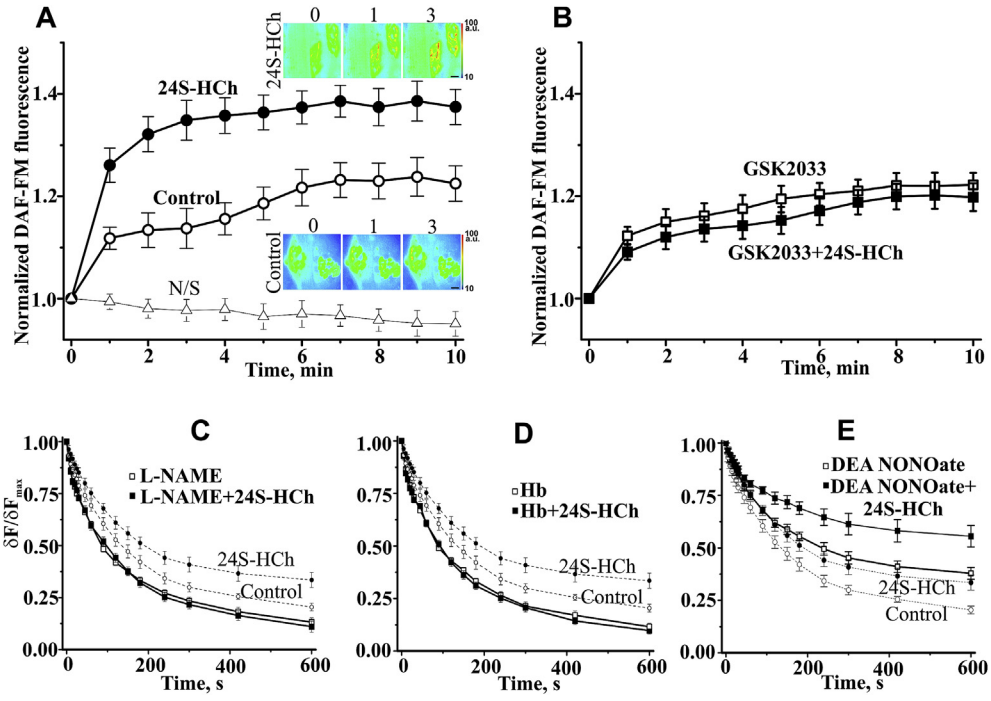

Fig. 5. Implication of NO signaling in the effect of long-term treatment with 24S-HCh. A, B – Time course of DAF-FM fluorescence during 20 Hz stimulation. The fluorescence of DAF-FM tended to decrease with time in the resting conditions (a photobleaching curve, marked N/S, no stimulation). A 20 Hz stimulus train led to a rise of DAF-FM fluorescence intensity ("Control" curve). 24S-HCh enhanced the increase in DAF-FM fluorescence evoked by the stimulation (A). LXR inhibitor (GSK2033) prevented the effect of 24S-HCh on the DAF-FM fluorescence (B). A, B; Y-axis indicates normalized fluorescence intensity, where initial fluorescence intensity immediately before the stimulation was taken as 1.0. Pseudocolor images recorded at 0, 1 and 3 min of the stimulus train. The corresponding intensity scale is provided to the right (a.u.). Scale bars − 10 μm. C, D, E − Kinetics of FM1-43 unloading at 20 Hz stimulation. NO synthase antagonist (L-NAME; C) and extracellular NO chelator (Hb; D) increased the rate of FM1-43 unloading in response to the stimulation and suppressed the effect of 24S-HCh. E − In contrast, an exogenous NO donor (DEA NONOate) attenuated the FM dye loss during the stimulus train and potentiated the effect of 24S-HCh. C-E, The FM-1-43 unloadings in control and 24S-HCh-treated muscles (from Fig. 2B) are shown by dashed lines. Other details are as in Fig. 2.

cavtratin completely abolished it (n = 12 animals for each of these curves) (Fig. 6B). Cavtratin increased the rate of FM1-43 loss during 20 Hz stimulation (nerve terminal fluorescence decreased to 34.0 ± 1.4% by 3rd min of the stimulation; $P < 0.05$, n = 8 animals) and prevented the effect of 24S-HCh on FM1-43 unloading (n = 8 animals) (Fig. 6C).

One possible way for enhancement of NO production by 24S-HCh may be linked to an increase in expression of NOS in muscle fibers. Consistent with this proposal is that an inhibitor of protein synthesis cycloheximide completely prevented the 24S-HC-induced enhancement of NO synthesis during 20 Hz stimulation (n = 12 animals) (Fig. 6D). While cycloheximide by itself had no impact on the kinetics of DAF-FM fluorescence at 20 Hz activity (n = 12 animals). This suggests that up-regulation of NOS at protein level may cause the increase in NO production during 20 Hz stimulation in 24S-HCh-treated muscles.

Increased protein synthesis could be linked with an increase in gene expression. Motor nerve terminals do not contain nucleus and, thus, cannot produce mRNA; in muscle fibers gene expression and hence mRNA levels could be changed relatively fast which may be accompanied by corresponding changes in protein synthesis. The eNOS and nNOS gene expression in muscle was assessed by qRT-PCR (Fig. 6E; n = 6 mice for each group), which confirmed the increase in *nNos* and

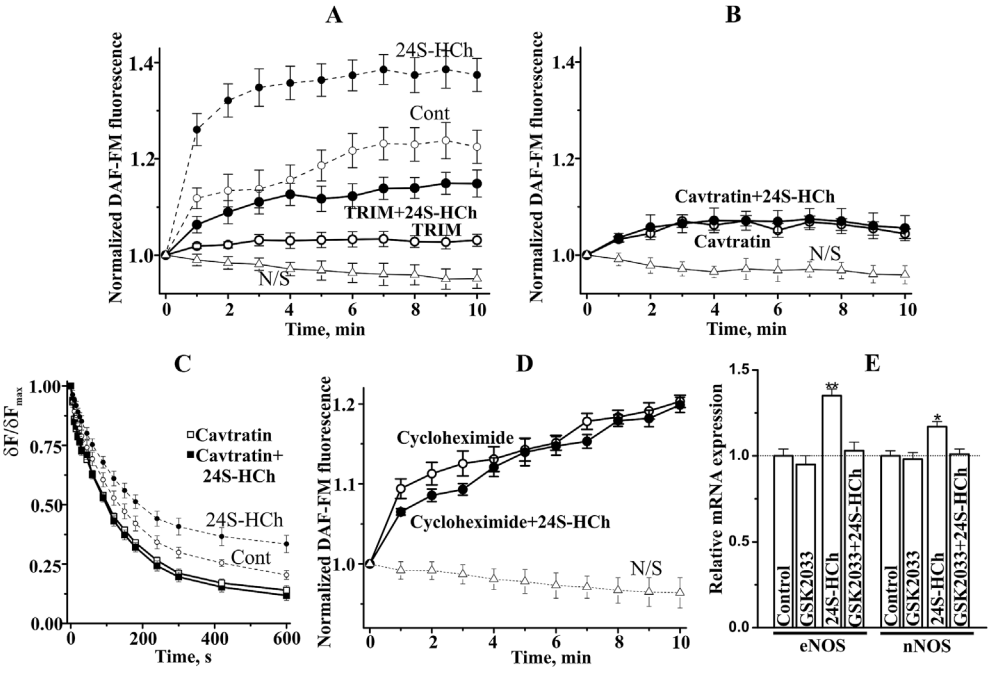

Fig. 6. NOS isoforms in the effects of 24S-HCh. (A) nNOS inhibitor (TRIM) suppressed the increase in DAF-FM fluorescence during 20 Hz stimulation both in 24S-HCh-treated and non-treated NMJs. Changes in DAF-FM fluorescence in control and 24S-HCh-treated muscles (from Fig. 5A) are indicated by dashed line. (B) Cell-permeable peptide derived from caveolin-1 (cavtratin) that mainly inhibits eNOS completely abolished the effect of 24S-HCh. (C) Time course of FM1-43 unloading at 20 Hz stimulation. Cavtratin increased the rate of FM1-43 unloading in response to the stimulation and prevented the effect of 24S-HCh. Changes in kinetics of FM1-43 loss in control and 24S-HCh-treated muscles (from Fig. 2B) are shown by dashed lines. (D) Protein synthesis inhibitor (cycloheximide) prevented the 24S-HCh-mediated increase in DAF-FM fluorescence. (E) Changes in expression of NOS. Evaluation by qRT-PCR indicates that 24S-HCh increased mRNA levels of *eNos* as well as *nNos*, and this action of the oxysterol was blocked by LXR antagonist (GSK2033). Other details are as in Fig. 5.

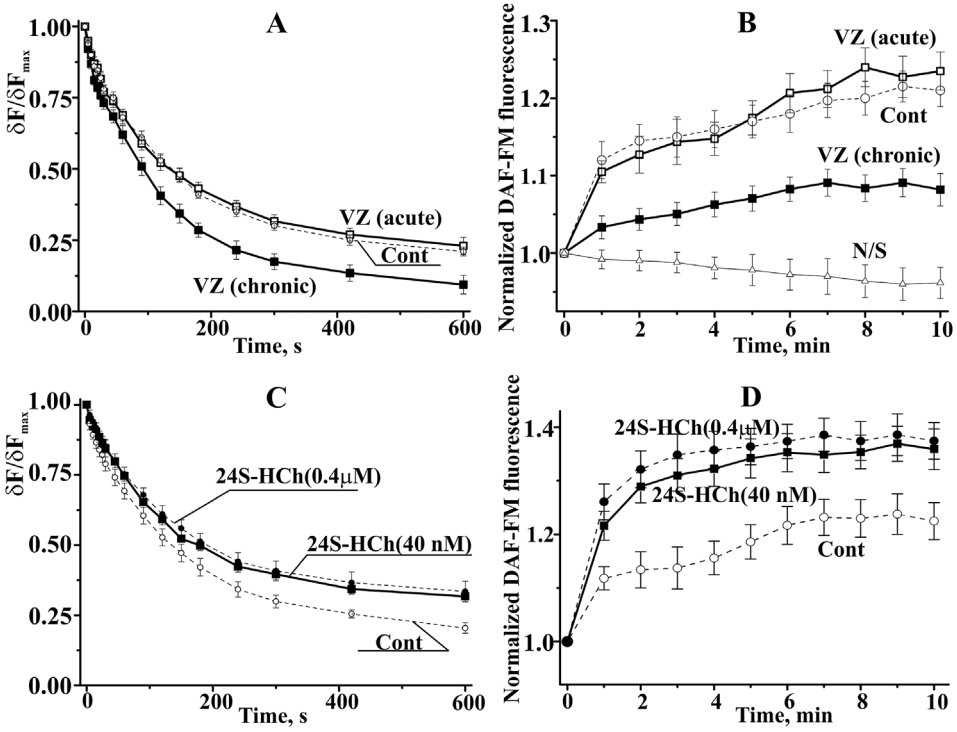

Fig. 7. Effects of treatment with CYP46A1 inhibitor voriconazole and with 24S-HCh at low concentration. Acute exposure of isolated muscles to voriconazole (1 μM, 2.5 h) did no change FM1-43 unloading (A) and DAF-FM fluorescence (B) during 20 Hz stimulation. In contrast, chronic treatment with voriconazole (60 mg/kg/day for 5 day) that decreases the plasma level of 24S-HCh accelerated the rate of FM1-43 unloading (A) and decreased the enhancement of DAF-FM fluorescence (B). 24S-HCh at low concentration (40 nM) decreased the rate of FM1-43 unloading (C) and promoted the increase in DAF-FM fluorescence (D) in response to 20 Hz stimulation. Changes in FM1-43 or DAF-FM fluorescence in control and 24S-HCh (0.4 μM)-treated muscles (from Fig. 2B or Fig. 5A, respectively) are indicated by dashed lines. Other details are as in Fig. 5.

eNos after treatment with 24S-HCh for 2.5 h. This enhancement of the gene expression was completely prevented by LXR inhibitor, whereas this inhibitor itself had no significant influence on the expression levels of *eNos* and *nNos*.

3.6. Effect of intraperitoneal administration of 24S-HCh-lowering drug and lower concentration of 24S-HCh on FM1-43 unloading and DAF-FM fluorescence

Chronic pretreatment mice with CYP46A1 inhibitor, voriconazole (with a Ki of 11 nM; intraperitoneally, 60 mg/kg/day for 5 days), that effectively decreases plasma level of 24S-HCh (Shafaati et al., 2010), had opposite influence on the FM1-43 unloading (n = 14 animals) and DAF-FM fluorescence (n = 14 animals) compared to the long-term action of 24S-HCh on the isolated muscles (Fig. 7A and B). Acute treatment of isolated muscles with voriconazole (1 μM, 2.5 h) had no effects on FM1-43 unloading (n = 14 animals) and DAF-FM fluorescence (n = 14 animals). These data suggest that the decrease in plasma content of 24S-HCh in voriconazol-treated mice was able to potentiate neuromuscular transmission via increasing synaptic vesicle exocytosis and decreasing NO synthesis. It is conceivable that presence of 24S-HCh in the circulation can tonically regulate the neuromuscular transmission. The plasma level of 24S-HCh in mice could be low than 0.4 μM (Shafaati et al., 2010), since we additionally tested effects of 40 nM 24S-HCh on FM1-43 unloading (n = 9 animals) and DAF-FM fluorescence (n = 9 animals) (Fig. 7C and D). At this low concentration, the magnitudes of the effects of 24S-HCh were similar to those of 0.4 μM 24S-HCh ($P > 0.05$). This suggests that these effects of 24S-HCh might depend upon a high affinity, but “low-capacity” mechanism.

4. Discussion

Studies in recent years have discovered the implication of oxysterols into cell to cell communications. Many signaling molecules, including G-protein coupled and nuclear receptors, ion channels and oxysterol-binding proteins, were identified as high affinity targets for different oxysterols (Lütjohann et al., 1996; Leoni and Caccia, 2013; Paul et al., 2013; Fumagalli M et al., 2017; Sytchev et al., 2017; Odnoshivkina et al., 2019). This suggests that oxysterol-dependent regulation has a pivotal role for adaptation of cellular events to alterations in cholesterol homeostasis and oxysterols can act in a para- or endocrine manner. Given that metabolic active central neurons are major producers of 24S-HCh appearing in the circulation, the possibility that 24S-HCh may provide an additional neurohumoral link between brain activity and skeletal muscle function looks attractive (Kasimov et al., 2017; Mukhutdinova et al., 2018).

Previously, we showed that relatively short (15–20 min) application of 24S-HCh potentiated neuromuscular transmission mainly due to enhancing recruitment of synaptic vesicles to exocytosis and the rate of their recycling at 20 Hz stimulation. This action of 24S-HCh depended on a decrease in NO production during the synaptic activity (Kasimov et al., 2017). In $SOD1^{G93A}$ mice the short treatment with 24S-HCh also suppressed the activity-induced NO synthesis at the NMJs that could be linked with an increase in the lipid raft integrity in junctional region (Mukhutdinova et al., 2018). Here, we found that prolongation of treatment with 24S-HCh resulted in an inversion of the exocytosis-promoting effect. The exposure to 24S-HCh for 2.5 h could attenuate an involvement of the synaptic vesicle to neurotransmitter release and decrease the rate of vesicular reuse at 20 Hz stimulation. This can explain a more profound depression of both EPP amplitudes and FM1-43 dye loss at 20 Hz motor nerve stimulation. Mechanism by which 24S-HCh affects synaptic vesicle mobilization is likely related to change in NO production in the synaptic region. This suggestion is supported by several lines of evidences. First, after treatment with 24S-HCh for 2.5 h, NO synthesis during 20 Hz-stimulation was upregulated in the junctional region, but not in extrajunctional compartment. Second, pharmacological inhibition of either eNOS (with cavtratin) or nNOS (with TRIM) completely or partially suppressed the 24S-HCh-mediated enhancement of NO production, respectively. Third, non-selective antagonist of NOS (L-NAME) as well as inhibitor of eNOS (cavtratin) prevented the decrease in the rate of FM1-43 dye unloading from the nerve terminals in 24S-HCh-treated muscles, while donor of NO potentiated this effect of 24S-HCh. Finally, hemoglobin, an extracellular NO scavenger, completely suppressed the 24S-HCh-mediated decrease in the rate of FM1-43 unloading. Therefore, 24S-HCh-mediated attenuation of synaptic vesicle exocytosis during 20 Hz stimulation may

be linked with the increased NO production mainly by eNOS at sites outside the motor nerve terminals (likely, in the muscle fibers). Local increase in NO production in the junctional region during 20 Hz stimulation in combination with abilities of hemoglobin and cavtratin (eNOS-binding peptide-concurrent of endogenous caveolins) to suppress the effect of 24S-HCh on FM1-43 unloading suggest that the source of NO is located in close vicinity of the postsynaptic membrane in muscle fiber. In many cells, eNOS can be recruited to plasma membrane by interaction with the raft-associated scaffold protein, caveolin. In rodent NMJs, caveolin 3 resides in postsynaptic region, where can serve as a scaffold for signaling molecules (Carlson et al., 2003; Hezel et al., 2010). Note that pretreatment of mice for 5 days with voriconazole (CYP46A1 inhibitor), decreased the plasma level of 24S-HCh (Shafaati et al., 2010), increased FM1-43 dye loss from synaptic vesicles and decreased NO production during 20 Hz activity in the NMJs. This suggests that endogenous 24S-HCh in the blood plasma might inhibit synaptic vesicle exocytosis and increase a NO synthesis in the NMJs. Further studies using genetic and pharmacological manipulations are required to identify whether endogenous 24S-HCh in the circulation may affect neuromuscular transmission.

The opposite effects of the short and long-term treatment with 24S-HCh may arise from a difference in receptors which are primary involved in these effects. Indeed, the action of short application of 24S-HCh was not modified by the LXR antagonist, while this compound completely abolished the attenuation of neurotransmitter release and synaptic vesicle exocytosis induced by 2.5 h exposure to 24S-HCh. This indicates that 24S-HCh can regulate neurotransmission at the NMJs via LXR stimulation. Nuclear LXRs α and β are expressed in skeletal muscle, where they are classically considered as regulator of metabolic homeostasis (Archer et al., 2014). Different types of muscle loading lead to an increase in generation of oxidized lipid agonists for LXRs, subsequent activation of LXRs may suppress inflammation, upregulate anti-oxidant defense and tune lipid metabolism, thereby preventing the muscle damage (Webb et al., 2017). Our data suggest that the stimulation of LXRs may also contribute to control the functional properties of NMJs. Given that increased level of acetylcholine promotes degeneration of NMJs, contributing to age-related motor deficit (Sugita et al., 2016), the LXR-dependent attenuation of the neurotransmitter release could have a potential protective action against the age-related structural/functional alterations of the NMJs.

The mechanism by which 24S-HCh-mediated LXR activation affects synaptic transmission at the NMJs is probably related to an increase in NO production during 20 Hz activity. Supporting this, an inhibition of LXRs suppressed the enhancement of NO synthesis induced by long-term exposure to 24S-HCh. LXRs can upregulate the NO-signaling via genomic and nongenomic pathways. Pharmacological stimulation of LXRs attenuated TNFα-evoked impairment of endothelium-dependent relaxation of aortic rings in response to acetylcholine via restoring NO bioavailability and increasing NO synthase expression (Spillmann et al., 2014). Activator of LXRs promoted the interaction of LXR β and estrogen receptor α within lipid rafts thereby initiating PI3K/Akt signaling pathway which leads to fast increase in NO production in the endothelial cells (Ishikawa et al., 2013). We believe that prolonged application of 24S-HCh could act on neurotransmission in the NMJs via transcriptional mechanism. Several evidences supported this view. First, 24S-HCh lost the ability to increase the NO production when protein synthesis was blocked with cycloheximide. Second, 24S-HCh increased mRNA of *eNos* and *nNos* which was prevented by LXR inhibitor. It is likely that 24S-HCh-induced LXR activation promoted the NOS expression in the muscle fibers. Third, prolonged application of even very low dose of 24S-HCh (40 nM) suppressed exocytosis and increased NO synthesis during 20 Hz stimulation. The proposal mechanism of LXR-dependent effects of 24S-HCh on NO signaling and neuromuscular transmission is provided on Fig. 8. Of course, we cannot exclude that the mechanism may be more complex and other possibilities, including depalmitoylation or some membrane dysfunction could affect recruitment of NOS to plasma membrane and, thus, contribute to effects of 2.5 h application of 24S-HCh.

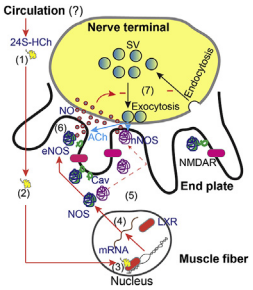

Fig. 8. Putative pathway for LXR-dependent effects of 24S-HCh on NO production and synaptic transmission in the mouse diaphragm. 24S-HCh (probably, from the circulation (1)) passes plasma membrane into cytoplasm (2), then the oxysterol activates LXR (a transcriptional factor) probably in muscle fibers (3). As a result of the LXR stimulation, expression of genes encoding eNOS and nNOS is increased (4), which is accompanied by increased protein levels of eNOS and nNOS (5). eNOS and nNOS are anchored in the postsynaptic region (end plate) and NOS activity is increased during synaptic transmission, leading to enhancement of NO production (6). The main source of the increased NO synthesis is likely eNOS, whose activity and location are dependent on interaction with caveolins. NO acting as a retrograde messenger suppresses acetylcholine (ACh) release at 20 Hz stimulation (7). This may occur due to an attenuation of synaptic vesicle mobilization to the sites of exocytosis and a decrease in rate of the vesicle recycling during activity. This proposal chain of events (1)–(7) is developed during at least a couple of hours and it is independent on activation of NDMA receptors. Schwann cell covered the nerve terminal is not shown, but it also contains nucleus and could potentially contribute to the effects of 24S-HCh.

The physiological or pathophysiological relevance of 24S-HCh-mediated suppression of neuromuscular transmission is unclear. Potentially, 24S-HCh could act as an endogenous tonic regulator of neuromuscular transmission by limiting synaptic overactivity, synaptic vesicle pool depletion, muscle force production and energy depletion during activity as well as degenerative structural alterations of NMJs. Indeed, elevated neurotransmitter release can aggravate degeneration of NMJs in aging and amyotrophic lateral sclerosis model mice (Sugita et al., 2016). The facts that 24S-HCh plasma levels were decreased in Niemann-Pick type C1 patients compared to healthy adult volunteers and were substantially lower than in children and adolescents (Bretillon et al., 2000; Sidhu et al., 2015) suggest possible negative effects of decrease in 24S-HCh on neuromuscular function. In the conditions accompanied by elevated levels of 24S-HCh (e.g. early stages of some neurodegenerative diseases, including Alzheimer's disease (Leoni and Caccia, 2013; Petrov et al., 2016)), 24S-HCh could serve as component of adaptive response, adjusting muscle activity to altered brain cholesterol metabolism.

5. Conclusion

The main findings of the present study are: that prolonged application of 24S-HCh suppresses synaptic vesicle exocytosis during 20 Hz activity at the NMJs; this action is dependent on both LXR activation and upregulation of NO-signaling (Fig. 8). These results raise the question of the possible relevance of brain-derived cholesterol metabolite 24S-HCh in the regulation of neuromuscular transmission via LXR/NOS signaling pathway. Limitation of our study is related to the use of pharmacological approaches, implying that further studies using molecular and genetic techniques are necessary to identify the precise molecular targets through which this oxysterol regulates the neuromuscular transmission.

Conflicts of interest

We declare no competing interests.

Author contributions

K. A. M, M.R.M., M.R.G. and G. F. Z. performed all experiments, data collection and analysis. A.M.P. interpreted results of experiments, designed and wrote the manuscript. All the authors read and approved the final version of manuscript.

Acknowledgements

This study was supported by the grant from Russian Foundation for Basic Research # 17-04-00046. We would like to thank the Reviewers for helpful comments and Morrie Lam (Harvard University) for carefully reading our manuscript.

Appendix A. Supplementary data

Supplementary data to this article can be found online at https://doi.org/10.1016/j.neuropharm.2019.03.018.

References

Archer, A., Laurencikiene, J., Ahmed, O., Steffensen, K.R., Parini, P., Gustafsson, J.Å., Korach-André, M., 2014. Skeletal muscle as a target of LXR agonist after long-term treatment: focus on lipid homeostasis. Am. J. Physiol. Endocrinol. Metab. 306 (5), E494–E502. https://doi.org/10.1152/ajpendo.00410.2013.

Babiker, A., Diczfalusy, U., 1998. Transport of side-chain oxidized oxysterols in the human circulation. Biochim. Biophys. Acta 1392, 333–339 PMID: 9630709.

Betz, W.J., Bewick, G.S., 1993. Optical monitoring of transmitter release and synaptic vesicle recycling at the frog neuromuscular junction. J. Physiol. 460, 287–309 PMID: 8387585.

Bigini, P., Steffensen, K.R., Ferrario, A., Diomede, L., Ferrara, G., Barbera, S., Salzano, S., Fumagalli, E., Ghezzi, P., Mennini, T., Gustafsson, J.A., 2010. Neuropathologic and biochemical changes during disease progression in liver X receptor beta-/- mice, a model of adult neuron disease. J. Neuropathol. Exp. Neurol. 69 (6), 593–605. https://doi.org/10.1097/NEN.0b013e3181df20e1.

Björkhem, I.1., Lütjohann, D., Breuer, O., Sakinis, A., Wennmalm, A., 1997. Importance of a novel oxidative mechanism for elimination of brain cholesterol. Turnover of cholesterol and 24(S)-hydroxycholesterol in rat brain as measured with 18O2 techniques in vivo and in vitro. J. Biol. Chem. 272 (48), 30178–30184.

Bretillon, L., Lütjohann, D., Ståhle, L., Widhe, T., Bindl, L., Eggertsen, G., Diczfalusy, U., Björkhem, I., 2000. Plasma levels of 24S-hydroxycholesterol reflect the balance between cerebral production and hepatic metabolism and are inversely related to body surface. J. Lipid Res. 41, 840–845 PMID: 10787445.

Carlson, B.M., Carlson, J.A., Dedkov, E.I., McLennan, I.S., 2003. Concentration of caveolin-3 at the neuromuscular junction in young and old rat skeletal muscle fibers. J. Histochem. Cytochem. 51 1113e1118. PMID: 12923236.

Cui, W., Taub, D.D., Gardner, K., 2007. qPrimerDepot: a primer database for quantitative real time PCR. Nucleic Acids Res. 35, D805–D809. https://doi.org/10.1093/nar/gkl767. Database issue.

Fumagalli, M., Lecca, D., Coppolino, G.T., Parravicini, C., Abbracchio, M.P., 2017. Pharmacological properties and biological functions of the GPR17 receptor, a potential target for neuro-regenerative medicine. Adv. Exp. Med. Biol. 1051, 169–192. https://doi.org/10.1007/5584_2017_92.

Hezel, M., de Groat, W.C., Galbiati, F., 2010. Caveolin-3 promotes nicotinic acetylcholine receptor clustering and regulates neuromuscular junction activity. Mol. Biol. Cell 21, 302e310. https://doi.org/10.1091/mbc.E09-05-0381.

Ishikawa, T., Yuhanna, I.S., Umetani, J., Lee, W.R., Korach, K.S., Shaul, P.W., Umetani, M., 2013. LXRβ/estrogen receptor-α signaling in lipid rafts preserves endothelial integrity. J. Clin. Investig. 123 (8), 3488–3497. https://doi.org/10.1172/JCI66533.

Janowski, B.A.1., Grogan, M.J., Jones, S.A., Wisely, G.B., Kliewer, S.A., Corey, E.J., 1999. Mangelsdorf DJ. Structural requirements of ligands for the oxysterol liver X receptors LXRalpha and LXRbeta. Proc. Natl. Acad. Sci. U.S.A. 96 (1), 266–271. https://doi.org/10.1073/pnas.96.1.266.

Kasimov, M.R., Giniatullin, A.R., Zefirov, A.L., Petrov, A.M., 2015. Effects of 5α-cholestan-3-one on the synaptic vesicle cycle at the mouse neuromuscular junction. Biochim. Biophys. Acta 1851, 674–685. https://doi.org/10.1016/j.bbalip.2015.02.012.

Kasimov, M.R., Zakyrjanova, G.F., Giniatullin, A.R., Zefirov, A.L., Petrov, A.M., 2016. Similar oxysterols may lead to opposite effects on synaptic transmission: olesoxime versus 5α-cholestan-3-one at the frog neuromuscular junction. Biochim. Biophys. Acta 1861, 606–616. https://doi.org/10.1016/j.bbalip.2016.04.010.

Kasimov, M.R., Fatkhrakhmanova, M.R., Mukhutdinova, K.A., Petrov, A.M., 2017. 24S-Hydroxycholesterol enhances synaptic vesicle cycling in the mouse neuromuscular junction: implication of glutamate NMDA receptors and nitric oxide. Neuropharmacology 117, 61–73. https://doi.org/10.1016/j.neuropharm.2017.01.030.

Leoni, V., Caccia, C., 2013. 24S-hydroxycholesterol in plasma: a marker of cholesterol turnover in neurodegenerative diseases. Biochimie 95, 595–612. https://doi.org/10.1016/j.biochi.2012.09.025.

Lütjohann, D., Breuer, O., Ahlborg, G., Nennesmo, I., Sidén, A., Diczfalusy, U., Björkhem, I., 1996. Cholesterol homeostasis in human brain: evidence for an age-dependent flux of 24S-hydroxycholesterol from the brain into the circulation. Proc. Natl. Acad. Sci. U.S.A. 93, 9799–9804 PMID: 8790411.

Maeno-Hikichi, Y., Polo-Parada, L., Kastanenka, K.V., Landmesser, L.T., 2011. Frequency-dependent modes of synaptic vesicle endocytosis and exocytosis at adult mouse neuromuscular junctions. J. Neurosci. 31 (3), 1093–1105. https://doi.org/10.1523/JNEUROSCI.2800-10.2011.

Mukhutdinova, K.A., Kasimov, M.R., Giniatullin, A.R., Zakyrjanova, G.F., Petrov, A.M., 2018. 24S-hydroxycholesterol suppresses neuromuscular transmission in SOD1(G93A) mice: a possible role of NO and lipid rafts. Mol. Cell. Neurosci. 88, 308–318. https://doi.org/10.1016/j.mcn.2018.03.006.

Odnoshivkina, U.G., Sytchev, V.I., Starostin, O., Petrov, A.M., 2019. Brain cholesterol metabolite 24-hydroxycholesterol modulates inotropic responses to β-adrenoceptor stimulation: the role of NO and phosphodiesterase. Life Sci. 220, 117–126. https://doi.org/10.1016/j.lfs.2019.01.054.

Paul, S.M., Doherty, J.J., Robichaud, A.J., Belfort, G.M., Chow, B.Y., Hammond, R.S., Crawford, D.C., Linsenbard, t A.J., Shu, H.J., Izumi, Y., Mennerick, S.J., Zorumski, C.F., 2013. The major brain cholesterol metabolite 24(S)-hydroxycholesterol is a potent allosteric modulator of N-methyl-D-aspartate receptors. J. Neurosci. 33, 17290–17300. https://doi.org/10.1523/JNEUROSCI.2619-13.2013.

Petrov, A.M., Giniatullin, A.R., Sitdikova, G.F., Zefirov, A.L., 2008. The role of cGMP-dependent signaling pathway in synaptic vesicle cycle at the frog motor nerve terminals. J. Neurosci. 28, 13216–13222. https://doi.org/10.1523/JNEUROSCI.2947-08.2008.

Petrov, A.M., Kasimov, M.R., Zefirov, A.L., 2016. Brain cholesterol metabolism and its defects: linkage to neurodegenerative diseases and synaptic dysfunction. Acta Naturae 8, 58–73 PMID: 27099785.

Ramirez, D.M., Andersson, S., Russell, D.W., 2008. Neuronal expression and subcellular localization of cholesterol 24-hydroxylase in the mouse brain. J. Comp. Neurol. 507 (5), 1676–1693. https://doi.org/10.1002/cne.21605.

Ribchester, R.R., Mao, F., Betz, W.J., 1994. Optical measurements of activity-dependent membrane recycling in motor nerve terminals of mammalian skeletal muscle. Proc. Biol. Sci. 255, 61–66. https://doi.org/10.1098/rspb.1994.0009.

Russell, D.W., Halford, R.W., Ramirez, D.M., Shah, R., Kotti, T., 2009. Cholesterol 24-hydroxylase: an enzyme of cholesterol turnover in the brain. Annu. Rev. Biochem. 78, 1017–1040. https://doi.org/10.1146/annurev.biochem.78.072407.103859.

Shafaati, M., Mast, N., Beck, O., Nayef, R., Heo, G.Y., Björkhem-Bergman, L., Lütjohann, D., Björkhem, I., Pikuleva, I.A., 2010. The antifungal drug voriconazole is an efficient inhibitor of brain cholesterol 24S-hydroxylase in vitro and in vivo. J. Lipid Res. 51, 318–323. https://doi.org/10.1194/jlr.M900174-JLR20.

Sidhu, R., Jiang, H., Farhat, N.Y., Carrillo-Carrasco, N., Woolery, M., Ottinger, E., Porter, F.D., Schaffer, J.E., Ory, D.S., Jiang, X., 2015. A validated LC-MS/MS assay for quantification of 24(S)-hydroxycholesterol in plasma and cerebrospinal fluid. J. Lipid Res. 56, 1222–1233. https://doi.org/10.1194/jlr.D058487.

Slater, C.R., 2017. The structure of human neuromuscular junctions: some unanswered molecular questions. Int. J. Mol. Sci. 18 (10), E2183. https://doi.org/10.3390/ijms18102183.

Spillmann, F., Van Linthout, S., Miteva, K., Lorenz, M., Stangl, V., Schultheiss, H.P., Tschöpe, C.4., 2014. LXR agonism improves TNF-α-induced endothelial dysfunction in the absence of its cholesterol-modulating effects. Atherosclerosis 232 (1), 1–9. https://doi.org/10.1016/j.atherosclerosis.2013.10.001.

Sugita, S., Fleming, L.L., Wood, C., Vaughan, S.K., Gomes, M.P., Camargo, W., Naves, L.A., Prado, V.F., Prado, M.A., Guatimosim, C., Valdez, G., 2016. VAChT overexpression increases acetylcholine at the synaptic cleft and accelerates aging of neuromuscular junctions. Skeletal Muscle 6, 31. https://doi.org/10.1186/s13395-016-0105-7.

Sun, M.Y., Taylor, A., Zorumski, C.F., Mennerick, S., 2017. 24S-hydroxycholesterol and 25-hydroxycholesterol differentially impact hippocampal neuronal survival following oxygen-glucose deprivation. PLoS One 12 (3), e0174416. https://doi.org/10.1371/journal.pone.0174416.

Sytchev, V.I., Odnoshivkina, Y.G., Ursan, R.V., Petrov, A.M., 2017. Oxysterol, 5α-cholestan-3-one, modulates a contractile response to β2-adrenoceptor stimulation in the mouse atria: involvement of NO signaling. Life Sci. 188, 131–140. https://doi.org/10.1016/j.lfs.2017.09.006.

Vanier, M.T., 2010. Niemann-Pick disease type C. Orphanet J. Rare Dis. 5, 16. https://doi.org/10.1186/1750-1172-5-16.

Webb, R., Hughes, M.G., Thomas, A.W., Morris, K., 2017. The ability of exercise-associated oxidative stress to trigger redox-sensitive signalling responses. Antioxidants 6 (3), E63. https://doi.org/10.3390/antiox6030063.